On the mechanism of bandgap formation in locally resonant finite elastic metamaterials

Christopher Sugino,[1] Stephen Leadenham,[1] Massimo Ruzzene,[1,2] and Alper Erturk[1,a)]
[1]*G.W. Woodruff School of Mechanical Engineering, Georgia Institute of Technology, Atlanta, Georgia 30332, USA*
[2]*D. Guggenheim School of Aerospace Engineering, Georgia Institute of Technology, Atlanta, Georgia 30332, USA*

(Received 20 June 2016; accepted 12 September 2016; published online 3 October 2016)

Elastic/acoustic metamaterials made from locally resonant arrays can exhibit bandgaps at wavelengths much longer than the lattice size for various applications spanning from low-frequency vibration/sound attenuation to wave guiding and filtering in mechanical and electromechanical devices. For an effective use of such locally resonant metamaterial concepts in finite structures, it is required to bridge the gap between the lattice dispersion characteristics and modal behavior of the host structure with its resonators. To this end, we develop a novel argument for bandgap formation in finite-length elastic metamaterial beams, relying on the modal analysis and the assumption of infinitely many resonators. We show that the dual problem to wave propagation through an infinite periodic beam is the modal analysis of a finite beam with an infinite number of resonators. A simple formula that depends only on the resonator natural frequency and total mass ratio is derived for placing the bandgap in a desired frequency range, yielding an analytical insight and a rule of thumb for design purposes. A method for understanding the importance of a resonator location and mass is discussed in the context of a Riemann sum approximation of an integral, and a method for determining the optimal number of resonators for a given set of boundary conditions and target frequency is introduced. The simulations of the theoretical framework are validated by experiments for bending vibrations of a locally resonant cantilever beam. *Published by AIP Publishing.*
[http://dx.doi.org/10.1063/1.4963648]

I. INTRODUCTION

It is a well understood phenomenon that metamaterials made from locally resonating[1] periodic structures (unlike phononic crystals[2] based on *Bragg scattering*) can exhibit *bandgaps* at wavelengths much longer than the lattice size to enable low-frequency vibration attenuation, wave guiding, and filtering, among other applications.[3] These *elastic/acoustic metamaterials* demonstrate broadband vibration damping characteristics; for example, beams bearing a sufficient number of tuned mass absorbers will form a bandgap.[4–6]

Liu *et al.*[1] first demonstrated locally resonant acoustic metamaterials that display bandgaps at lattice scales two orders of magnitude smaller than the wavelength, opening a new avenue in acoustic metamaterials research. Ho *et al.*[7] explored a broadband attenuation in a locally resonant sonic crystal, using a rigid plastic frame with metal spheres embedded in a silicone rubber. Jensen[8] examined bandgaps in both 1D and 2D mass spring systems, considering the effects of damping and boundaries on the bandgap. Huang *et al.*[9] discussed the "negative effective mass density" effect that occurs in acoustic metamaterials, using both discrete and microstructure continuum models. Yu *et al.*[5] investigated a flexural bandgap in an Euler-Bernoulli beam using two degree-of-freedom (DOF) vibration absorbers. They used a transfer matrix approach to determine the expected bandgap and validated their model using both finite-element modeling and experiment. Sun *et al.*[4] performed a comprehensive study of an acoustic metamaterial theory, developing the wave theory for infinite periodic locally resonant beams and performing numerical studies for finite locally resonant beams. They found that, for high frequency excitation, boundary conditions or mode shapes are not important for the absorber behavior, but that lower frequency designs require consideration of the mode shapes of the structure. Since these studies for finite structures were purely numerical, it is difficult to gain insight into a specific design criterion. Xiao *et al.*[6] also examined flexural waves in beams with vibration absorbers, developing a set of analytical equations to locate the band edge frequencies, validating their approach with experiment and finite-element modeling. Pennec *et al.*[10] investigated a thin plate with periodic cylindrical stubs, showing that the band structure depends on the thickness of the plate and the height of the stubs. Oudich *et al.*[11] demonstrated a low frequency, local resonance-based bandgap on a thin plate using deposited stubs. They studied their system using the finite element method (FEM) and a unit cell based analysis. Employing the same local resonance principle, Oudich *et al.*[12] modeled a waveguide that can guide a single mode in a plate. Assouar *et al.*[13] tested a plate-type locally resonant metamaterial using silicone rubber-tungsten composite stubs. Achaoui *et al.*[14] examined the local resonance bandgap and demonstrated that it was resilient to random arrangements, whereas the Bragg

a)Author to whom correspondence should be addressed. Electronic mail: alper.erturk@me.gatech.edu

bandgap was not. Moving towards a more adaptable metamaterial, Wang *et al.*[15] demonstrated a tunable locally resonant acoustic metamaterial using buckled elements, allowing the bandgap to be tuned by varying the applied load. Peng and Pai[16] analyzed an acoustic metamaterial plate, presenting a design guideline for the locally resonant bandgap.

Wave-type arguments for bandgap formation rely on the assumptions of traveling waves and an infinite structure made from a repeated unit cell, such that no standing waves form. However, in finite structures, the dynamic response is determined by the mode shapes of the structure. In this work, we present a modal analysis approach to bandgap formation in locally resonant finite metamaterial beams as one-dimensional waveguides. In an effort to gain an analytical insight, we employ and validate an assumption of infinite absorbers on the finite structure. We then provide a simple design guideline for placing the bandgap at a desired frequency range, present an experimental validation case, and draw comparisons to the canonical single degree-of-freedom tuned mass absorber.

II. MODAL ANALYSIS OF A BANDGAP FORMATION

Consider a uniform Euler-Bernoulli beam with arbitrary boundary conditions with bending stiffness EI, linear mass density (i.e., mass per length) m, and length L. The beam has a transverse base motion $w_b(t)$ with relative transverse vibrations $w(x,\ t)$, such that the absolute displacement is $w_{abs}(x,t) = w_b(t) + w(x,t)$. In addition, the beam experiences some distributed external loading per unit length $f(x,\ t)$. Without a loss of generality, we assume that the system is undamped, with the understanding that modal damping can be easily introduced later. Assume there are S undamped spring-mass absorbers attached to the beam at locations x_j, with masses m_j, stiffnesses k_j, natural frequencies $\omega_{a,j}^2 = k_j/m_j$, and relative displacements u_j, for $j = 1 \ldots S$. A representative schematic showing a locally resonant cantilever beam under a base excitation is shown in Fig. 1.

Under these conditions, the governing equation for the beam in physical coordinates is

$$EI\frac{\partial^4 w}{\partial x^4} + m\frac{\partial^2 w}{\partial t^2} - \sum_{j=1}^{S} m_j \omega_{a,j}^2 u_j(t)\delta(x - x_j) = f(x,t) - m\ddot{w}_b(t), \tag{1}$$

where $\delta(x)$ is the Dirac delta function. The governing equation for each resonator is

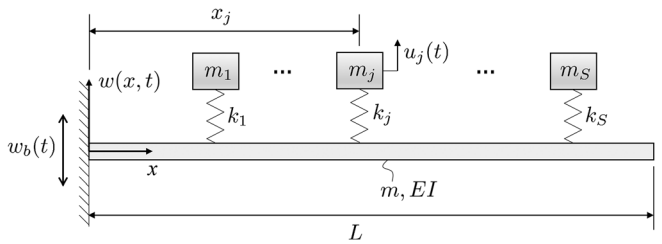

FIG. 1. A schematic of a locally resonant metamaterial beam under base excitation (in the absence of the distributed force $f(x,\ t)$ in Eq. (1)). Cantilever (fixed-free) boundary conditions are shown as a typical example.

$$\ddot{u}_j(t) + \omega_{a,j}^2 u_j(t) + \frac{\partial^2 w}{\partial t^2}(x_j,t) = -\ddot{w}_b(t). \tag{2}$$

Assume that the natural frequencies ω_i and mode shapes $\phi_i(x)$ of the plain beam (i.e., the beam without resonators) are known and that the mode shapes are normalized such that

$$\int_0^L \phi_i(x)\phi_j(x)dx = L\delta_{ij}, \tag{3}$$

where δ_{ij} is the Kronecker delta.

Using an assumed-modes expansion with N terms and employing the corresponding plain beam mode shapes as basis functions, we assume

$$w(x,t) = \sum_{k=1}^{N} \phi_k(x)\eta_k(t). \tag{4}$$

Substituting Eq. (4) into Eqs. (1) and (2), applying orthogonality (see Meirovitch[17] for more details), and rearranging provide the governing equations in modal coordinates

$$\sum_{i=1}^{N}\left[\delta_{ik} + \sum_{j=1}^{S}\hat{m}_j\phi_i(x_j)\phi_k(x_j)\right]\ddot{\eta}_i(t) + \sum_{j=1}^{S}\hat{m}_j\phi_k(x_j)\ddot{u}_j(t) + \omega_k^2\eta_k(t) = -\ddot{w}_b(t)\left(\int_0^L \phi_k(x)dx + \sum_{j=1}^{S}\hat{m}_j\phi_k(x_j)\right) + \frac{1}{mL}\int_0^L f(x,t)\phi_k(x)dx, \tag{5}$$

$$\ddot{u}_j(t) + \omega_{a,j}^2 u_j(t) + \sum_{i=1}^{N}\ddot{\eta}_i(t)\phi_i(x_j) = -\ddot{w}_b(t), \tag{6}$$

where $\hat{m}_j = m_j/(mL)$ is the jth normalized resonator mass, and it is assumed that the free indices k and j go from 1 to N and 1 to S, respectively.

Equations (5) and (6) form a system of $N+S$ coupled second order ordinary differential equations, which can be solved in a variety of ways. Importantly, it is possible to obtain the approximate resonant frequencies and mode shapes of the entire structure by solving an eigenvalue problem. This provides little analytical insight, as the eigenvalue problem must be solved numerically. Instead, assuming everything is harmonic at some excitation frequency ω, using an overbar to indicate amplitude, Eq. (6) can be solved for the absorber amplitudes

$$\bar{u}_j = \frac{\omega^2}{\omega_{a,j}^2 - \omega^2}\sum_{i=1}^{N}\bar{\eta}_i\phi_i(x_j) + \frac{\omega^2}{\omega_{a,j}^2 - \omega^2}\bar{w}_b. \tag{7}$$

Then, substituting Eq. (7) into Eq. (5), we obtain

$$(\omega_k^2 - \omega^2)\bar{\eta}_k - \omega^2\sum_{i=1}^{N}\sum_{j=1}^{S}\frac{\hat{m}_j\omega_{a,j}^2}{\omega_{a,j}^2 - \omega^2}\phi_i(x_j)\phi_k(x_j)\bar{\eta}_i = \bar{Q}_k, \tag{8}$$

where

$$\bar{Q}_k = \frac{1}{mL}\int_0^L \bar{f}(x)\phi_k(x)dx + \bar{w}_b\omega^2\left(\frac{1}{L}\int_0^L \phi_k(x)dx + \sum_{j=1}^{S}\frac{\hat{m}_j\omega_{a,j}^2}{\omega_{a,j}^2-\omega^2}\phi_k(x_j)\right). \quad (9)$$

Assuming the natural frequencies of the absorbers to be identical at some target frequency ω_t, Eq. (8) simplifies to

$$\left(\omega_k^2-\omega^2\right)\bar{\eta}_k - \frac{\omega_t^2\omega^2}{\omega_t^2-\omega^2}\sum_{i=1}^{N}\sum_{j=1}^{S}\hat{m}_j\phi_i(x_j)\phi_k(x_j)\bar{\eta}_i = \bar{Q}_k. \quad (10)$$

This system of equations cannot be readily solved for a simple analytical expression for the modal weightings $\bar{\eta}_k$ due to the coupling terms from the presence of the vibration absorbers. However, for a sufficiently large S, assuming the attachment locations x_j and masses m_j are sufficiently well distributed, the following approximation can be employed:

$$\sum_{j=1}^{S}\hat{m}_j\phi_i(x_j)\phi_k(x_j) \approx \frac{\mu}{L}\int_0^L \phi_i(x)\phi_k(x)dx = \mu\delta_{ik}, \quad (11)$$

where

$$\mu = \sum_{j=1}^{S}\hat{m}_j \quad (12)$$

determines the ratio of added mass (of the absorbers) to the mass of the plain beam. If the attachment locations and masses are evenly distributed, the approximation becomes

$$\sum_{j=1}^{S}\frac{1}{S}\phi_i(x_j)\phi_k(x_j) \approx \frac{1}{L}\int_0^L \phi_i(x)\phi_k(x)dx = \delta_{ik}, \quad (13)$$

a right-sided Riemann sum approximation of the integral. This sum becomes exact in the limit as $S \to \infty$:

$$\lim_{S\to\infty}\sum_{j=1}^{S}\frac{1}{S}\phi_i(x_j)\phi_k(x_j) = \frac{1}{L}\int_0^L \phi_i(x)\phi_k(x)dx = \delta_{ik}. \quad (14)$$

This "infinite absorbers" assumption is the modal analysis analogue to the wave theory assumption of an infinitely long beam composed of repeated unit cells. Provided there are a sufficient number of attachments on the beam, Eq. (13) becomes a good approximation, as will be discussed later. With this significant simplification, Eq. (10) can be solved explicitly for $\bar{\eta}_k$ with a closed-form expression

$$\bar{\eta}_k = \frac{\bar{Q}_k}{\omega_k^2-\omega^2\left(1+\frac{\mu\omega_t^2}{\omega_t^2-\omega^2}\right)}. \quad (15)$$

Note that, under the assumption of Eq. (13), a similar simplification can be made to the modal forcing due to base excitation, i.e.,

$$\sum_{j=1}^{S}\hat{m}_j\phi_k(x_j) \approx \frac{\mu}{L}\int_0^L \phi_k(x)dx \quad (16)$$

such that the modal forcing is given by

$$\bar{Q}_k = \frac{1}{mL}\int_0^L \bar{f}(x)\phi_k(x)dx + \bar{w}_b\omega^2\left(1+\frac{\mu\omega_t^2}{\omega_t^2-\omega^2}\right)\frac{1}{L}\int_0^L \phi_k(x)dx. \quad (17)$$

It can be shown that

$$\lim_{\omega\to\omega_t}\bar{\eta}_k(\omega_t) = -\frac{\bar{w}_b}{L}\int_0^L \phi_k(x)dx. \quad (18)$$

For the cantilever beam excited only by base motion, this is sufficient to ensure that $|\bar{w}_{abs}(L)|$ is very small at ω_t, as will be evident in later numerical studies. In the absence of base excitation (i.e., $\bar{w}_b = 0$), $\bar{\eta}_k(\omega_t) = 0$, an antiresonance that is present for every mode shape, resulting in zero displacement everywhere on the beam. This is the continuous system analogue to a perfectly tuned undamped vibration absorber in a single-degree-of-freedom system.

Rearranging Eq. (15) yields

$$\bar{\eta}_k = \frac{\bar{Q}_k\left(\omega_t^2-\omega^2\right)}{\omega_k^2\left(\omega_t^2-\omega^2\right)-\omega^2\left(\omega_t^2(1+\mu)-\omega^2\right)}. \quad (19)$$

The roots of the polynomial in the denominator give the new resonant frequencies associated with each mode. Much like a single vibration absorber splits a single resonance into two new resonances, the presence of an infinite number of absorbers on the continuous structure of the beam splits the resonance of every mode shape. Let the excitation frequency and the plain beam natural frequencies be normalized by the attachment natural frequency ω_t, such that $\hat{\omega} = \omega/\omega_t$ and $\Omega_k = \omega_k/\omega_t$. The two positive roots of the denominator are then

$$\hat{\omega}^+ = \sqrt{\frac{1+\mu+\Omega_k^2}{2}\left(1+\sqrt{1-\frac{4\Omega_k^2}{\left(1+\mu+\Omega_k^2\right)^2}}\right)}, \quad (20)$$

$$\hat{\omega}^- = \sqrt{\frac{1+\mu+\Omega_k^2}{2}\left(1-\sqrt{1-\frac{4\Omega_k^2}{\left(1+\mu+\Omega_k^2\right)^2}}\right)}. \quad (21)$$

Both of these resonant frequencies are shown as a function of Ω_k in Fig. 2 for illustration using a total absorber mass to plain beam mass ratio of unity (i.e., $\mu = 1$).

The limiting values of these frequencies give an insight into the formation of the bandgap. The higher resonance $\hat{\omega}^+$ has a minimum value of $\sqrt{1+\mu}$ at $\Omega_k = 0$ and then increases with Ω_k without bound, approaching $\hat{\omega}^+ = \Omega_k$ as $\Omega_k \to \infty$. The lower resonance $\hat{\omega}^-$ has a minimum value of 0 when $\Omega_k = 0$ and then asymptotically approaches $\hat{\omega} = 1$

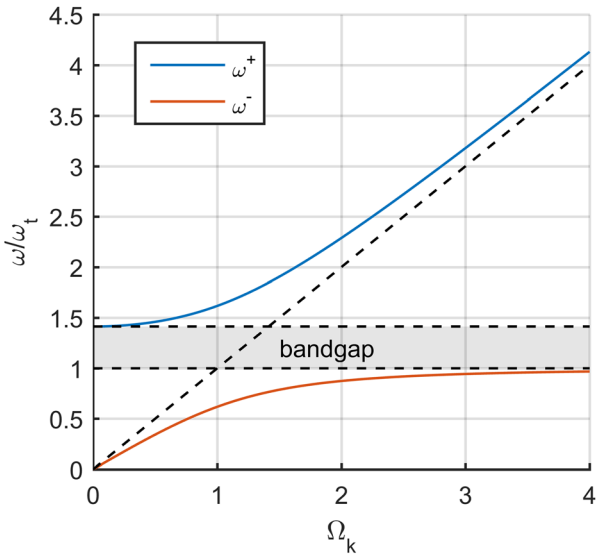

FIG. 2. New resonant frequencies as a function of original resonant frequency for $\mu = 1$. The bandgap corresponds to the region with no resonances between the two horizontal lines at $\omega/\omega_t = 1$ and $\omega/\omega_t = \sqrt{1+\mu}$.

as $\Omega_k \to \infty$. Thus, the new resonances associated with each mode can never be in the frequency range

$$\omega_t < \omega < \omega_t\sqrt{1+\mu}. \tag{22}$$

This frequency range defines the limits of the bandgap and provides an easy method for locating the bandgap at a desired frequency range. This agrees with the result given by Peng and Pai,[16] where they found the bandgap edge frequencies in a plate with attached resonators, using a unit cell level analysis. This type of assumed mode analysis can easily be extended to any canonical continuous vibrating structure with vibration absorbers. The bandwidth of the bandgap is determined by the mass ratio and attachment frequencies, given by

$$\Delta\omega = \omega_t(\sqrt{1+\mu} - 1). \tag{23}$$

The bandgap of attenuation bandwidth $\Delta\omega$ can be centered at some frequency ω_c by making the attachment natural frequencies

$$\omega_t = \frac{2\omega_c}{1+\sqrt{1+\mu}}. \tag{24}$$

Note that the foregoing discussion of the infinite-absorber bandgap edge frequencies has no dependence on the type of excitation or the boundary conditions of the beam. The only property of the beam that affects the bandgap bandwidth is the total mass, as it directly changes the mass ratio μ. The boundary conditions and bending stiffness of the beam *will* affect the exact shape of the transmissibility, even in the infinite-absorber case. Furthermore, as can be seen in Fig. 2, the values of Ω_k for the specific boundary conditions and bending stiffness will affect how close $\hat{\omega}^+$ are to the upper bound of the bandgap. For ω_t values that are large relative to the fundamental of the original beam, there will be less separation between the upper bound of the bandgap and the first resonance after the bandgap. For ω_t values that are small relative to the fundamental frequency of the beam, there will be more separation between the upper bound of the bandgap and the first resonance after the bandgap.

This simplification also allows a quick calculation of the deformed shape of the beam for large values of N, since there is no need to solve a linear system of equations or an eigenvalue problem. A typical metric for vibration performance of a structure (especially, in the base excitation scenarios) is transmissibility, defined as

$$TR(\omega) = \left|\frac{\bar{w}(x_{out})}{\bar{w}(x_{in})}\right| = \left|\frac{\sum_{i=1}^{N}\phi_i(x_{out})\bar{\eta}_i(\omega)}{\sum_{i=1}^{N}\phi_i(x_{in})\bar{\eta}_i(\omega)}\right|. \tag{25}$$

This is simple to calculate numerically as a function of ω, since we know the expression for $\bar{\eta}_i(\omega)$. This allows us to generate heat maps of transmissibility as functions of excitation frequency ω and input location x_{in} for some fixed x_{out} very rapidly, producing graphs such as shown in Fig. 3, which characterizes the dynamic response of the full structure.

III. MODEL VALIDATION

The assumed modes model used above was validated with both the finite element method (FEM) and a simple experiment. The FEM model for the beam was developed using a one-dimensional mesh and beam elements. A comparison between the FEM and assumed-modes simulation results for a cantilever beam undergoing a base excitation is shown in Fig. 4.

To validate the assumed modes model, experiments were performed with a vertical aluminum cantilever under a base excitation. The absorbers comprised of small spring steel cantilevers with tip masses attached to the main structure with magnets. The base acceleration was measured using a Kistler piezoelectric accelerometer, and the tip velocity was measured using a laser Doppler vibrometer (LDV). The base excitation was achieved with a long stroke shaker and an amplifier. The experimental setup is shown as an inset in Fig. 5.

The vibration absorbers were tuned to create a bandgap around ω_2. A comparison of the model and experiment is shown in Fig. 5. Note that, to fully model the system as

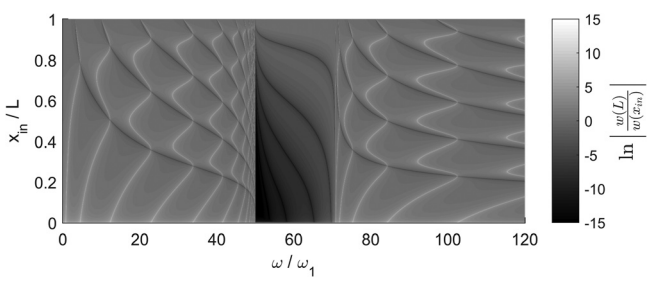

FIG. 3. Tip transmissibility versus point force input location x_{in} and excitation frequency for a cantilever beam bearing an infinite number of vibration absorbers, $\mu = 1$, $\omega_t = 50\omega_1$, $N = 50$.

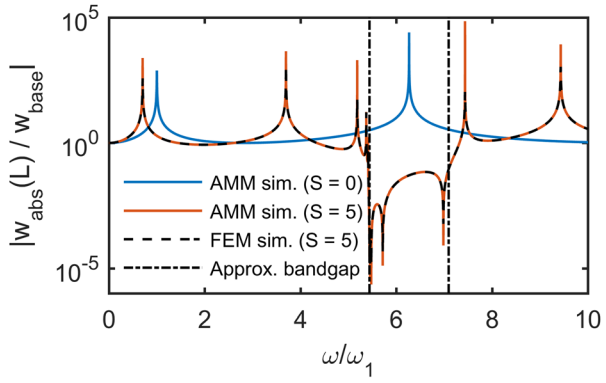

FIG. 4. A comparison of the assumed-modes method (AMM) and FEM transmissibilities for a cantilever beam undergoing base excitation, $S = 5$, $\mu = 0.7$, $\omega_t = 0.868\omega_2$. The bandgap approximation with an infinite number of absorbers ($S \to \infty$) is also shown for reference.

shown, it was necessary to add point masses to the assumed modes formulation described earlier. This is a simple change to implement, since point masses affect the mass matrix in a similar fashion to the absorber masses, without the frequency dependence. In addition, modal damping is introduced to the model easily in order to capture the finite resonant amplitudes. There was a good agreement between the model and experimental results, although the bandgap is not very prominent, since the target frequency is very low, and the total absorber mass is not high (yielding a low μ value).

IV. EVALUATING THE INFINITE ABSORBER APPROXIMATION

One of the perceived shortcomings of a wave-type analysis of the bandgaps in finite structures is the loss of information regarding mode shapes, such as the potential drawbacks of placing a vibration absorber near a node of a mode shape. The formulation presented here provides a way to understand how both the absorber mass distribution and spatial distribution affect the bandgap.

The key approximation made is the Riemann sum

$$\sum_{j=1}^{S} \hat{m}_j \phi_i(x_j)\phi_k(x_j) \approx \frac{\mu}{L}\int_0^L \phi_i(x)\phi_k(x)dx. \tag{26}$$

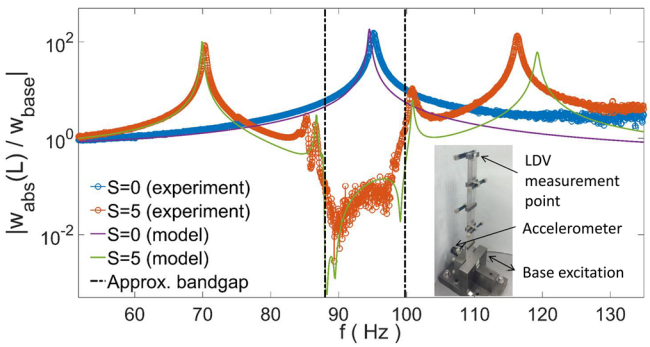

FIG. 5. A comparison of the experimental results and assumed modes model simulations. The bandgap approximation with an infinite number of absorbers ($S \to \infty$) is also shown for reference. The inset shows the experimental setup of a vertical cantilever with five absorbers as a locally resonant metamaterial beam under base excitation.

The convergence behavior of the approximation as S becomes large can be seen by looking at the transmissibility and resonant frequencies as a function of S. This is visualized in Fig. 6 for evenly spaced attachments on a cantilever beam undergoing base excitation with a mass ratio of $\mu = 1$, targeting a frequency of $\omega_t = 50\omega_1$. It is clear that, by $S = 13$, the bounds on the bandgap agree well with the ideal infinite-absorber case. This suggests that, even though the derivation was only exact in the limit as $S \to \infty$, the approximation is sufficiently good for design purposes once S becomes sufficiently large.

The accuracy of this approximation depends on not only the mode shapes under consideration and, consequently, the boundary conditions of the beam but also the absorber locations x_j and the absorber masses m_j. However, it is not trivial to determine which modes are most important for a given target frequency or how good the approximation needs to be for the bandgap to appear. There is a significant qualitative difference in modal weightings in the fully decoupled and coupled cases. Under the infinite absorber assumption, each modal weighting has only two resonant frequencies, and the resonant frequencies of each mode are distinct. When the modal weightings are fully coupled, each mode shows all of the resonances of the structure, regardless of how lightly coupled the modes are. It is possible to reduce the error in the sum for a particular set of modes and attachment locations by varying the mass distribution, but this would not be the optimal arrangement for another set of modes. To gain some insight into the approximation error, consider a mass distribution of the form

$$m_j = \mu m \Delta x_j, \tag{27}$$

where Δx_j is the size of the interval before the jth absorber. In this case, the approximation becomes a right Riemann sum,

$$\sum_{j=1}^{S} \Delta x_j \phi_i(x_j)\phi_k(x_j) \approx \int_0^L \phi_i(x)\phi_k(x)dx, \tag{28}$$

such that the Riemann sum error is bounded by the expression

$$|Error| \le \frac{L}{2}\max_{[0,L]}\left|\frac{d}{dx}(\phi_i(x)\phi_k(x))\right|(\Delta x_j)_{max}. \tag{29}$$

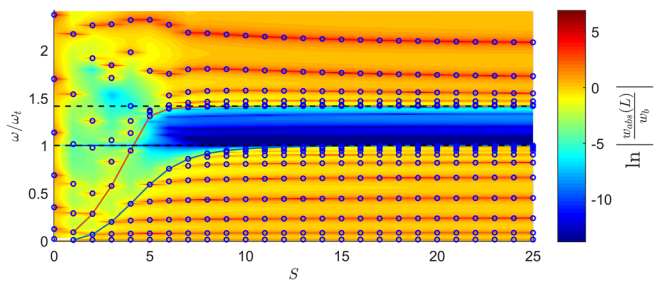

FIG. 6. Transmissibility (tip displacement/base displacement) and resonant frequencies for a cantilever undergoing base excitation versus S, $\mu = 1$, $\omega_t = 50\omega_1$, $N = 50$. Small circles indicate natural frequencies, the heatmap shows the transmissibility, dashed lines show the infinite absorber bandgap, and the two solid lines track ω_{S+1} and ω_S.

This upper bound on the error will become larger for higher modes, because the maximum slope will tend to be larger. This means not only that more absorbers will be necessary to reduce the error in the approximation for higher target frequencies but also that having more absorbers will reduce the error for any type of boundary conditions. Thus, if it is known in advance that a structure will experience an excitation in a certain frequency band, the natural frequency and mass ratio for the absorbers can be chosen using Eq. (22), and the number of absorbers can be chosen to be sufficiently high such that the exact boundary conditions or type of excitation will not significantly affect the bandgap.

V. OPTIMAL NUMBER OF RESONATORS FOR A FINITE STRUCTURE

The formulation described in this work provides a simple way to choose an "optimal" number of resonators for a given type of beam. Reconsider Fig. 6 which shows transmissibility and resonant frequencies as a function of the number of attachments. It is evident that the bandgap forms between the resonant frequencies ω_S and ω_{S+1}, assuming the resonant frequencies are sorted in an ascending order. The separation $\omega_{S+1} - \omega_S$ is shown as a function of S in Fig. 7.

It is clear that the separation converges to $\Delta\omega$ as S becomes large, as defined in Eq. (23). Interestingly, certain values of S give a greater bandwidth than the infinite-absorber case, and there is a value S_{opt} (here $S=5$), which gives the greatest separation of resonances around the bandgap. Note that the corresponding bandwidth may actually be smaller than the corresponding single-absorber bandwidth, but it provides a clear design guideline for a "bandgap-like" region of vibration reduction. The optimal value S_{opt} depends on not only the mass ratio μ and the target frequency ω_t but also the boundary conditions and excitation of the system under consideration. Alternatively, if the level of vibration reduction is the primary concern, a similar method can be used to optimize for a minimum average transmissibility across the bandgap or to minimize the maximum transmissibility in the bandgap.

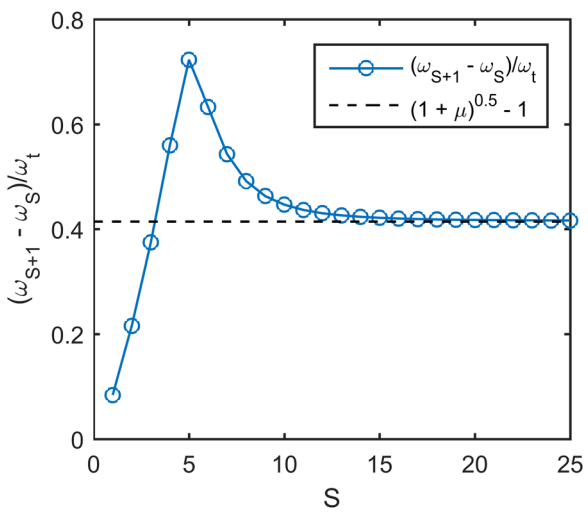

FIG. 7. Separation of resonant frequencies on the boundaries of the bandgap versus S, $\mu=1$, $\omega_t = 50\omega_1$, and $N=50$.

VI. COMPARISON TO A SINGLE ABSORBER

It is useful to compare the bandgap-type results described in Sections II–V to the canonical one degree-of-freedom (DOF) vibration absorber. The canonical vibration absorber, as described by Den Hartog,[18] consists of a single damped oscillator attached to an undamped 1-DOF host structure. In this case, the separation of the fixed points in the transmissibility gives a measure of bandwidth that we can compare to the bandwidth given in Eq. (23). Den Hartog shows that the normalized frequencies of the fixed points are governed by

$$g^4 - 2g^2\frac{1+f^2+\mu f^2}{2+\mu} + \frac{2f^2}{2+\mu} = 0, \tag{30}$$

where $g = \omega/\Omega_n$, $f = \omega_a/\Omega_n$, $\mu = m/M$, Ω_n is the resonant frequency of the host structure, ω_a is the absorber natural frequency, and m and M are the masses of the absorber and host structure, respectively. For an absorber tuned exactly to the resonance of the main structure, $f=1$, giving fixed points

$$g = \sqrt{1 \pm \sqrt{\frac{\mu}{\mu+2}}}. \tag{31}$$

As $\mu \to \infty$, one of the fixed points approaches zero, and the other approaches $\sqrt{2}$. The separation of the fixed points is simply

$$\Delta g = \sqrt{1+\sqrt{\frac{\mu}{\mu+2}}} - \sqrt{1-\sqrt{\frac{\mu}{\mu+2}}}. \tag{32}$$

There are two reasonable ways to compare this bandwidth to the bandwidth of the bandgap in Eq. (22). First, the attachment frequencies can be taken to be fixed at the same value ω_a regardless of mass ratio, in which case the bandwidth is

$$\Delta g = \sqrt{1+\mu} - 1, \tag{33}$$

which increases without bound as μ increases. Alternatively, the bandgap could be centered at the same frequency ω_a, taking the mass ratio into account, in which case the bandwidth is

$$\Delta g = \frac{2\left(\sqrt{1+\mu}-1\right)}{1+\sqrt{1+\mu}}, \tag{34}$$

which asymptotically approaches $\Delta g = 2$ as $\mu \to \infty$. Note that keeping the bandgap centered at a certain frequency with the increasing mass ratio requires a decrease in the attachment natural frequencies. These different bandwidths are shown in Fig. 8 as functions of mass ratio.

For a single absorber or bandgap centered at ω_a, the bandwidth is limited simply because the lower bound approaches $\omega = 0$. In this case, a single absorber will almost always result in a greater bandwidth, except for prohibitively large mass ratios. However, if we keep the attachment natural frequency fixed, adding mass will increase the bandgap bandwidth much more than it will increase the single absorber bandwidth.

This is not a perfect comparison for a variety of reasons. For a single degree of freedom system, it is assumed that the absorber is targeting the resonant frequency of the system.

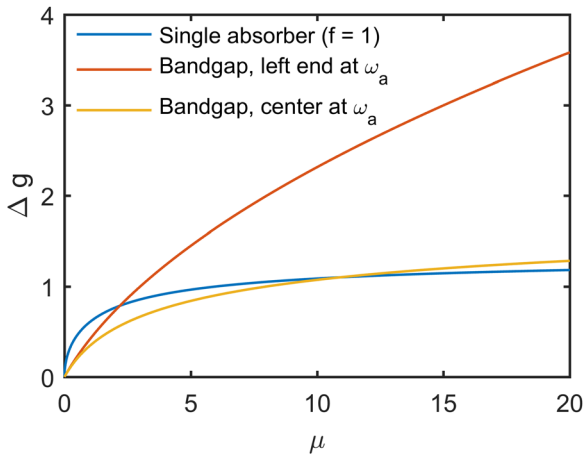

FIG. 8. A comparison of bandwidth versus mass ratio curves for a single absorber, bandgap, and centered bandgap.

The bandgap has no such restriction and can be placed without considering the dynamic characteristics of the original structure. Furthermore, there are practical limitations in the Den Hartog absorber setting, such as the fact that vibration levels of a single absorber may not be allowable in realistic scenarios, due to space and material limitations, among others.

VII. CONCLUSIONS

Locally resonant elastic/acoustic metamaterials result in bandgaps at wavelengths much longer than the lattice size for low-frequency vibration/sound attenuation, wave guiding, and filtering, among other applications. We presented modal analysis justification for bandgap formation in finite beams with locally resonating attachments and prescribed boundary conditions by bridging the gap between the lattice dispersion characteristics in infinite media and modal behavior of the overall finite structure. It was shown that the dual problem to wave propagation through an infinite periodic beam is the modal analysis of a finite beam with an infinite number of vibration absorbers. A simple formula that depends only on the absorber natural frequency and total mass ratio was derived for placing the bandgap in a desired frequency range, which can provide a quick rule of thumb for design purposes, provided a sufficient number of absorbers are used. A method for understanding the importance of an absorber location and a mass was discussed in the context of a Riemann sum approximation of an integral, and a method for determining the optimal number of resonators for a given set of boundary conditions and target frequency was introduced. This analysis can be readily extended to other types of locally resonant materials, such as rods or plates.

ACKNOWLEDGMENTS

This work was supported by the Air Force Office of Scientific Research Grant No. FA9550-15-1-0397 "Integrated multi-field resonant metamaterials for extreme, low frequency damping" monitored by Dr. B. L. Lee.

[1]Z. Liu, X. Zhang, Y. Mao, Y. Y. Zhu, Z. Yang, C. T. Chan, and P. Sheng, Science **289**, 1734 (2000).
[2]W. Cheng, J. Wang, U. Jonas, G. Fytas, and N. Stefanou, Nat. Mater. **5**, 830 (2006).
[3]V. Laude, *Phononic Crystals*, De Gruyter Studies in Mathematical Physics (Walter de Gruyter GmbH, Berlin, Germany, 2015), Vol. 26.
[4]H. Sun, X. Du, and P. F. Pai, J. Intell. Mater. Syst. Struct. **21**, 1085 (2010).
[5]D. Yu, Y. Liu, H. Zhao, G. Wang, and J. Qiu, Phys. Rev. B **73**, 064301 (2006).
[6]Y. Xiao, J. Wen, D. Yu, and X. Wen, J. Sound Vib. **332**, 867 (2013).
[7]K. M. Ho, C. K. Cheng, Z. Yang, X. X. Zhang, and P. Sheng, Appl. Phys. Lett. **83**, 5566 (2003).
[8]J. S. Jensen, J. Sound Vib. **266**, 1053 (2003).
[9]H. H. Huang, C. T. Sun, and G. L. Huang, Int. J. Eng. Sci. **47**, 610 (2009).
[10]Y. Pennec, B. Djiafari-Rouhani, H. Larabi, J. O. Vasseur, and A. C. Hladky-Hennion, Phys. Rev. B **78**, 104105 (2008).
[11]M. Oudich, M. Senesi, M. B. Assouar, M. Ruzzene, J.-H. Sun, B. Vincent, Z. Hou, and T.-T. Wu, Phys. Rev. B **84**, 165136 (2011).
[12]M. Oudich, M. B. Assouar, and Z. Hou, Appl. Phys. Lett. **97**, 193503 (2010).
[13]M. B. Assouar, M. Senesi, M. Oudich, M. Ruzzene, and Z. Hou, Appl. Phys. Lett. **101**, 173505 (2012).
[14]Y. Achaoui, V. Laude, S. Benchabane, and A. Khelif, J. Appl. Phys. **114**, 104503 (2013).
[15]P. Wang, F. Casadei, S. Shan, J. C. Weaver, and K. Bertoldi, Phys. Rev. Lett. **113**, 014301 (2014).
[16]H. Peng and P. F. Pai, Int. J. Mech. Sci. **89**, 350 (2014).
[17]L. Meirovitch, *Principles and Techniques of Vibrations* (Prentice-Hall, Inc., Upper Saddle River, NJ, 1997).
[18]J. P. Den Hartog, *Mechanical Vibrations*, 4th ed. (McGraw-Hill Book Company Inc., New York, NY, 1956).